Металлофиз. новейшие технол. / *Metallofiz. Noveishie Tekhnol.*
2018, т. 40, № 12, сс. 1649–1673/ DOI: 10.15407/mfint.40.12.1649
Оттиски доступны непосредственно от издателя
Фотокопирование разрешено только
в соответствии с лицензией

PACS numbers: 61.43.Gt, 61.72.Ff, 64.75.-g, 68.35.Ct, 68.35.Dv, 68.35.Fx, 81.15.Pq

Influence of Copper Pretreatment on the Phase and Pore Formations in the Solid Phase Reactions of Copper with Tin

V. V. Morozovych, A. R. Honda, Yu. O. Lyashenko, Ya. D. Korol, O. Yu. Liashenko, C. Cserhati*, and A. M. Gusak

Bohdan Khmelnytsky National University of Cherkasy,
81 Shevchenko Blvd.,
UA-18031 Cherkasy, Ukraine
**University of Debrecen,*
1 Egyetem Ter.,
H-4032 Debrecen, Hungary

The solid-phase reactions of copper with tin are considered, and the porosity of the reaction products depending on the pretreatment of the copper substrate is investigated. Copper substrates for the reaction are prepared by electrodeposition of copper layers with thickness of up to 100 microns on the rolled copper plates. The defects of substrates are determined by the different modes of electrodeposition—stationary, reversible, and stochastic ones. As shown, the thicknesses of the intermediate phases, their ratio, the number and spatial distribution of pores in the reaction products significantly depend on the mode of electrodeposition. The statistical dependences of the pore distribution along and across the interface as well as the characteristics of the roughness of the interface are revealed.

Key words: copper–tin interface, diffusion, solid-state reactions, electrodeposition, defects, pore formation, pinning.

Розглядаються твердофазні реакції міді з циною, та досліджується пористість продуктів реакції в залежності від попереднього оброблення мідного підложжя. Мідні підложжя для реакції готуються шляхом електроосадження прошарків міді товщиною до 100 мкм на прокатані мідні пла-

Corresponding author: V. V. Morozovych
E-mail: vladmorozua@gmail.com

Citation: V. V. Morozovych, A. R. Honda, Yu. O. Lyashenko, Ya. D. Korol, O. Yu. Liashenko, C. Cserhati, and A. M. Gusak , Influence of Copper Pretreatment on the Phase and Pore Formations in the Solid Phase Reactions of Copper with Tin, *Metallofiz. Noveishie Tekhnol.*, **40**, No. 12: 1649–1673 (2018), DOI: 10.15407/mfint.40.12.1649.

тівки. Дефектність підложжя визначається різними режимами електроосадження: стаціонарним, реверсним і стохастичним. Показано, що товщини проміжних фаз, їх відношення, кількість і просторовий розподіл пор у продуктах реакції істотно залежать від режиму електроосадження. Виявлено статистичні залежності розподілу пор вздовж і поперек інтерфейсу, а також характеристики його шерсткости.

Ключові слова: інтерфейс мідь–цина, дифузія, твердофазні реакції, електроосадження, дефекти, пороутворення, пінінґування.

Рассматриваются твёрдофазные реакции меди с оловом, и исследуется пористость продуктов реакции в зависимости от предварительной обработки медной подложки. Медные подложки для реакции готовятся путём электроосаждения слоёв меди толщиной до 100 мкм на прокатанные медные пластинки. Дефектность подложек определяется различными режимами электроосаждения: стационарным, реверсивным и стохастическим. Показано, что толщины промежуточных фаз, их соотношение, количество и пространственное распределение пор в продуктах реакции существенно зависят от режима электроосаждения. Установлены статистические зависимости распределения пор вдоль и поперёк интерфейса, а также характеристики его шероховатости.

Ключевые слова: интерфейс медь–олово, диффузия, твёрдофазные реакции, электроосаждение, дефекты, порообразование, пиннинг.

(Received November 16, 2018)

1. INTRODUCTION

One of the most common reasons for chip failure is due to the soldered copper/tin based contacts, that is, the soldered contacts are the weakest part of the chip [1, 2] and this is related, in particular, to the pore formation in the contact zone. The temperature range is from room temperature up to 250°C (typical range of packaging and operation of the integrated circuits). In the solid phase reaction of copper with tin, only two phases Cu_6Sn_5 (η-phase) and Cu_3Sn (ε-phase) grow. In the process of soldering, when the tin-based solder is liquid, the growth of the scallop-like Cu_6Sn_5 phase is dominant, which occurs due to the rapid diffusion of copper along liquid channels between the scallops [3–6]. In this case, the formation of Cu_3Sn phase layer during the first second is generally suppressed, and then occurs, but much slower than the growth of Cu_6Sn_5 [7]. At the stage of operation, when the solder is solid (solid-state ageing), the growth rate of both phases becomes approximately the same [8]. The pore formation with the growth of Cu_3Sn phase is the main reason for the failure of the soldered contacts. The cause of pore formation is the flow of vacancies in the direction of copper, which arises as a result of the fact that, in the process of mutual diffusion through the specified phase, copper diffuses much faster

than tin. As a result, vacancies are accumulated on the interface of Cu_3Sn/Cu and form a chain of pores. Since the difference of the component mobility and the corresponding vacancy flux towards, the faster component generates Kirkendall's effect (the lattice flow as a whole); that pore formation is known to be Kirkendall voiding in the Anglo-Saxon literature. It is commonly called the Frenkel effect in the journals of the former USSR. The ways to fight the Frenkel effect have been looking for a long time. The oldest method known to us was proposed by the group of Geguzin, in the 1970's being associated with the use of full compression [9, 10]. Namely, the supersaturation of vacancies can be relaxed in two main ways: (1) the annihilation of vacancies at boundary dislocations (K-sinks), which leads to the creep of the dislocation and corresponding motion of atomic planes, that is to Kirkendall's effect, and (2) the combination of vacancies in the pores (F-sinks) without the motion of planes (Frenkel effect). Mathematical aspects of competition between two types of sinks are described, in particular, in [11, 12].

The idea of Geguzin's team was simple: the suppression of F-sinks by the pressure of several dozen atmospheres. As Geguzin and coauthors showed, such pressures are sufficient to suppress pore formation, but not sufficient for a significant decrease in the diffusion rate. Indeed, in the experiments [9, 10] on copper/nickel alloy at a pressure of less than a hundred atmospheres, pores were almost suppressed, and the speed of Kirkendall's effect increased approximately twice. Unfortunately, in the formation and operation of chips, the application of full compression is unrealistic, and therefore, other ways of suppression are looked for. For example, pore formation may be reduced, if nickel is added to copper [13]. Another interesting way is the use of nanotwinned copper [14], which can diminish pore formation. However, the preparation of nanotwinned coating on copper is a rather expensive and specific process. Therefore, the searches continue, and the task of influencing on pore formation remains relevant.

It is intuitively clear that preprocessing of copper or the deposition of additional layers of copper can affect the reaction of copper and tin in various ways. There are, at least, 3 reasons for this as follow.

1. If an additional density of dislocations is formed as a result of processing in copper, then, extra vacancies in the vicinity of the interfacial boundary of the ε-phase/copper receive additional K-sinks, on which they can disappear without pore formation [15].

2. On the other hand, processing, which leads to an increase of the dislocation density, usually simultaneously leads to a decrease of the grain size, that is, to an increase of the density of triple joints of grain boundaries. Triple joints can serve as centres for heterogeneous pore formation.

3. Different types of processing leave a different roughness of the

interface, including the average amplitude and the average length of the 'bends' of future interfaced boundary.

In works [16, 17], the technology of obtaining layers of copper electrodeposited in stationary, pulsed reverse and stochastic modes on copper substrates was worked out. The application of the Chua generator model for nonlinear oscillations is described to construct a time series of stochastic voltage fluctuations on electrodes in the vicinity of two stationary values. Two values of the voltage of the electrodeposition, calculated from the polarization curve for the given conditions of electrodeposition, were applied for the experiment. While performing the work, a hardware-software complex (HSC) was created to control the electrolytic deposition process. The analysis of stationary and stochastic regime effect of electrolytic deposition on the structure of the obtained copper layers on copper substrates was carried out using x-ray diffraction analysis and scanning electron microscopy. The analysis of diffractograms shows that in the samples obtained after the stationary electrodeposition of copper, the size of the grains is smaller compared with the initial samples of the textured rolled copper. It is found that crystallites with the preferential orientation of planes (111) and the presence of crystallites with orientation (220) and (200), which are placed parallel to the surface of the sample, are formed in stationary electrodeposition modes. Electrodeposition in a pulsed reverse mode shows that the orientation of grain planes (220) prevails in these samples. In stochastic electrodeposition modes, an almost structurally perfect polycrystalline layer of copper is formed. In these samples, there is a full spectrum of the crystallite plane orientations (111), (220) and (200) in the same proportions, which is similar to the structure of powder copper.

Scanning electron microscopy shows that the grain structures of the stationary and stochastic modes of electrolytic deposition of copper layers differ substantially in their morphological structure [16, 17]. In the case of stochastic stress, the deposited layer of copper consists of rounded monodisperse grains. Under constant voltage of electrodeposition, both the grain of a lamellar structure and grains of irregular shape are formed much larger than in the case of the use of stochastic modes of voltage change. In addition, Ref. [17] points out that the structure type of the electrodeposited copper layers affects the growth result of intermediate phases during solid-phase reactions in the Cu–Sn system. This effect is studied in detail in this paper.

The structure effect of the electrodeposited copper on copper substrates under different current conditions on the result of solid phase reactions with tin is studied in the paper. The modes of copper deposition are described in Sec. 2. Copper coatings obtained under different modes of electrodeposition, are investigated using a scanning electron microscope (SEM) and x-ray structure analysis. Subsequently, the ob-

tained electrodeposited samples are immersed in the molten tin for a short time, and then, the obtained samples continue to anneal in solid state for hundreds of hours. As a result, the evolution of phase thickness, the shapes of interfaces, the number and distribution of pores are found and their characteristics, depending on the method of copper electrodeposition are compared (Section 3).

2. EXPERIMENT DESCRIPTION

The theory and technology of the stationary mode of electrodeposition with the use of constant voltage applied to the electrodes of the electrochemical cell are developed in the scientific literature in sufficient detail [18]. The stationary mode of electrodeposition has a number of disadvantages involving, for example, the uneven thickness of the electrically deposited films. This is due to the instability of the stationary mode of electrodeposition, when the protrusions formed by fluctuations on the electrodes lead to a decrease in the distance between them and, accordingly, to an increase in the flow of electrodeposition in these areas, which leads to even greater growth of the formed protrusions. Different types of heterogeneous electrodeposition modes are used to fight this phenomenon [19–24], such as pulsed mode, harmonic mode, reverse pulsed modes of electrodeposition. The most perfect surface coatings are obtained in the mode of the reverse pulsed electrodeposition, when the cathode and the anode periodically change places by changing the polarity of the current. The electrolytic deposition in this study was carried out in two stationary, slow and fast stochastic and pulsed reverse modes. Initially, according to the specified composition of the electrolyte, its temperature and sample sizes, a polarization curve was constructed experimentally, according to which the basic modes of electrodeposition were selected. For electrodeposition of copper layers on copper substrates in various stationary and non-stationary modes, the developed HSC [16, 17] was used that allowed to maintain a given voltage on the electrodes of an electrochemical cell in a real-time mode and to record the corresponding values of the current strength.

To implement the stochastic modes of electrodeposition, we used the model of the Chua generator [25–27], namely, the model of a dynamic system with the behaviour of a strange attractor. The application of this model allows obtaining continuous transitions of the voltage of electrodeposition between two stationary modes at random moments of time. The course of the stochastic process was calculated first by the methods of mathematical modelling, as a set of values of a random function in successive moments of time. Calculated in this way, the random function profile was restored in the HSC at two different time scales. Two corresponding stochastic regimes (slow and fast) differed

only in the time scale, in this case, by 500 times. The slow stochastic regime corresponded to such a change in the voltage at the electrodes with the time, when the polarization of the electrodes occurred faster than the change in voltage over time. In this case, the functional dependences of stresses and current forces are connected by a polarization curve determined in stationary conditions. In this case, the functional dependences of the stresses and current strength are connected by a polarization curve determined in stationary conditions. And, conversely, in a fast stochastic mode, the process of unsteady electrodeposition occurred without such an adjustment of the current strength to instant voltage values.

2.1. Sample Preparation

The process of electrodeposition was carried out on the copper substrate of 1 mm thickness. The surfaces of the copper plates were partially insulated to provide a surface area of 1 cm^2. The copper plates used for electrodeposition and polarization curve construction were grinded and polished using grinding SiC paper (P180, P1200, P2400). After polishing, the copper plates were purified in an ultrasonic bath with ethanol for 100 seconds. After ultrasonic cleaning, the copper plates were homogenized by annealing at a temperature of 550°C for 2 hours in an argon atmosphere. Prior to electrodeposition, the samples were further purified by electrochemical etching in an electrolyte, maintaining the distance between the anode and the cathode of 5 cm. The sample was subtracted for 10 minutes at a voltage $U = 0.21$ V (current density was $j = 0.022$ A/cm^2). Then, plates of copper were rinsed in water. On the cleared copper plates, the copper layer was precipitated in stationary mode with current density $j = 0.022$ A/cm^2 for 10 minutes. For electrolytic deposition, we used an electrolyte of 0.36M $CuSO_4 \cdot H_2O + 1.22$M H_2SO_4 composition.

2.2. Construction of a Polarization Curve

In accordance with the given conditions of electrolysis (the size of the samples of 10×10 mm^2 and the distance between the cathode and the anode of 5 cm) in the galvanodynamic regime at a rate of 0.02 V/s, a polarization curve was constructed. The constructed polarization curve characterizes the deposition of copper on copper plates at a given concentration and temperature of the electrolyte and is shown in Fig. 1.

Based on the constructed polarization curve, the voltage intervals corresponding to the activated and diffusion mode of electrodeposition are determined. The stationary modes of electrodeposition were performed according to the parameters of points *1* and *2* in Fig. 1. The sto-

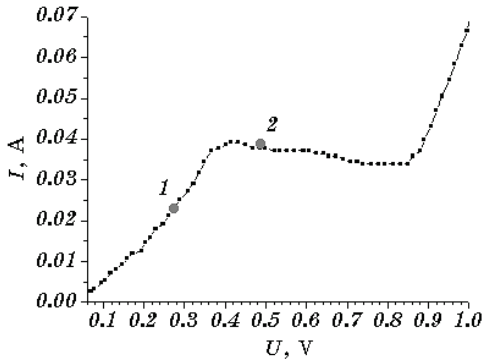

Fig. 1. Galvanodynamic polarization curve obtained at Cu electrodeposition.

chastic modes of electrodeposition were carried out using the model of the Chua's nonlinear oscillator generator when nonlinear voltage fluctuations were carried out in the vicinity of points 1 and 2 with random continuous transitions between them. In this case, the minimum voltage value was 0.17 V, maximum 0.56 V. At the first (0.24 V) and second (0.49 V) stationary points, the maximum variations in the amplitude of the voltage fluctuations were 0.07 V (see Fig. 2, *a*, *b*).

The control of deposition was carried out by means of fixing the total charge. In the experiments carried out, the value of the total passed charge $q = 86.54$ C was chosen. Considering the current output (it has been experimentally determined that for this electrolyte the current output was about 55%), this total charge corresponded to the mass of the sediment $m = 33$ mg, which corresponds to a thickness of about 100 microns in stationary modes of electrodeposition. The parameters of electrolytic deposition in the case of stochastic, pulsed reversal, and stationary modes are given in Table 1.

In the HSC, in each mode of electrodeposition, the corresponding time dependences of the voltage were introduced and the corresponding values of the current strength were measured. Figures 2, *a*–*e* show fragments of time dependences of voltage and current in the case of non-stationary modes.

The surfaces of the electrodeposited copper layers were investigated by means of scanning electron microscopy (see Fig. 3).

As seen from the micrographs, the surfaces obtained during the deposition in the first stationary (Sample 1) and reverse pulsed (Sample 5) modes are the most evenly filled with grains of copper precipitate (Fig. 3, *a*, *d*). The surfaces obtained in the second stationary mode and in both stochastic modes differ in the significant heterogeneity of grain placement and their associations and have a globular structure. It should be noted that the placement of globules in the second stationary mode is spatially heterogeneous. The globules themselves have sig-

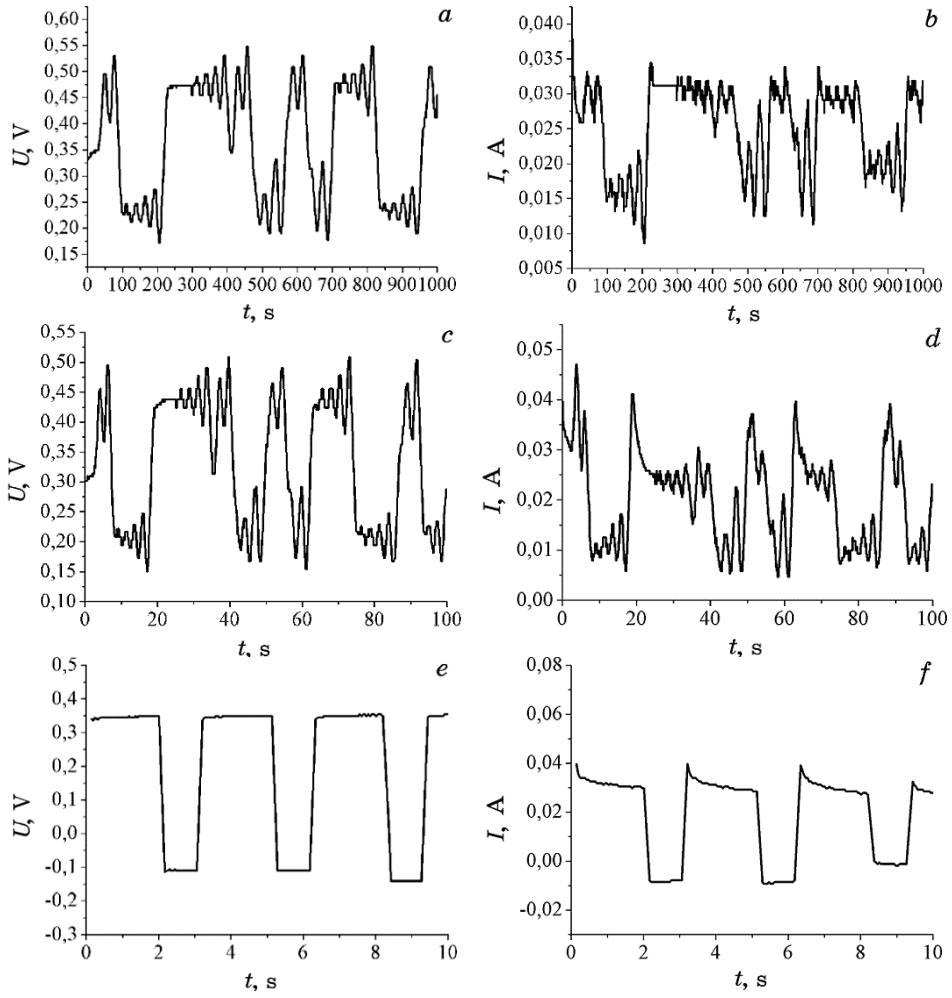

Fig. 2. Fragments of voltage and current time dependences in the case of: *a*, *b*—slow stochastic; *c*, *d*—fast stochastic; *e*, *f*—pulsed reverse modes of electrodeposition.

nificant variations in their size. The sediment globules, obtained in the stochastic modes, are more periodic and spatially homogeneous.

2.3. Integral Analysis of Defects

The methods of x-ray diffractometry were used to study the structural state of electrically deposited layers of copper obtained under different deposition conditions. The methods of analysing the defects of such layers are described in [17]. In general, defects are related to the aver-

TABLE 1. Parameters of electrodeposition.

No.	Deposition mode	Voltage U, V	Current density j, A/cm^2	$\Delta m/S$, kg/m^2	Deposition time, min
Sample 1	Stationary No. 1	0.24	0.0113	3.32	110
Sample 2	Stationary No. 2	0.499	0.0431	3.35	47
Sample 3	Slow stochastic (t = 1 s) (x_0 = 0.2, α = 7, β = 10 in Chua's model [16, 17])	U_{min} = = 0.17 U_{max} = = 0.56 U_{st} = 0.49 U_{st} = 0.24	j_{min} = 0.0138, j_{max} = 0.031	3.32	55
Sample 4	Fast stochastic (t = 20 ms) (x_0 = 0.2, α = 7, β = 10 in Chua's model [16, 17])	U_{min} = = 0.18 U_{max} = = 0.56 U_{st} = 0.49 U_{st} = 0.25	j_{min} = 0.010 j_{max} = 0.042	3.47	58
Sample 5	Pulse reversible (fill factor D = 0.66, τ = 3 s)	–0.119 +0.367	–0.0171 +0.0338	2.95	120

age density of deposition current. In our case, it is the smallest in reverse impulse deposition mode, increases in stationary mode (Sample 1) and is the largest in stationary (Sample 2) and in stochastic deposition modes. This is evident from the width of the diffraction lines on the diffractograms depicted in Fig. 4. In Figure 4, lines of diffractograms are set up to 100 units.

It is known that in the process of electrolytic deposition of a number of metals, an axial growth texture with a crystallographic axis being perpendicular to the surface of the sediment is formed [28, 29]. Methods for x-ray diffractometry were used to study the structural state of electrolytic copper coatings obtained under different deposition conditions. The obtained diffractograms (filtered FeK_α radiation) in comparison with the standard (annealed compressed copper powder) and a bar chart of the PDF-2 database are shown in Fig. 4. Relative intensities of diffraction peaks are presented in Table 2.

Qualitative analysis of diffractograms and data analysis of this Table shows that, in the conditions of a stochastic current, a near-polycrystalline precipitates with a slight tendency toward texture along the direction of <110> are formed. It can be noted that there is no significant influence on the orientational structural characteristics of the velocity of stochastic oscillations. In case of stationary deposition (constant current), regardless of the cathode potential, the texture (110) of the precipitate becomes sharper, as can be seen by increas-

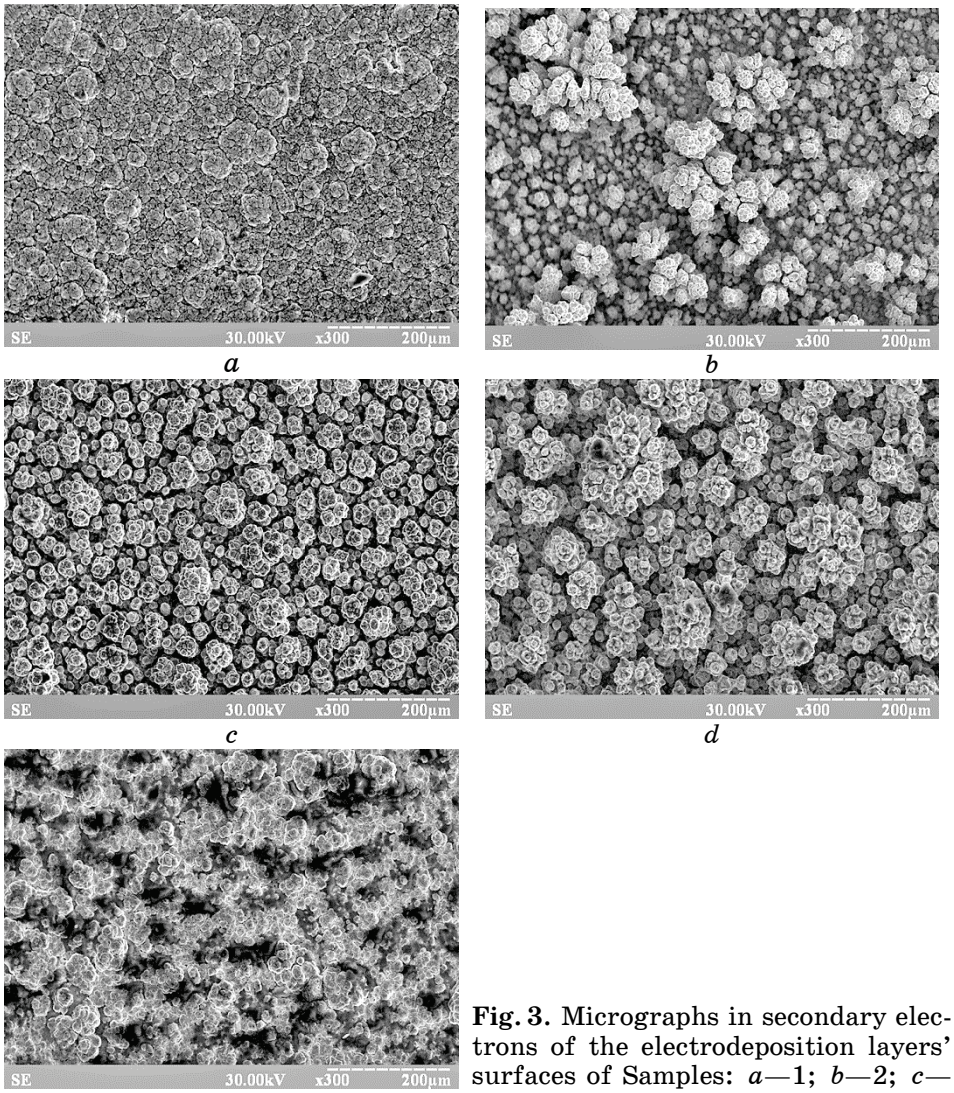

Fig. 3. Micrographs in secondary electrons of the electrodeposition layers' surfaces of Samples: *a*—1; *b*—2; *c*—3; *d*—4; *e*—5.

ing the relative intensity of the copper diffraction line (220). Under the pulsed reverse mode, the electrolytic precipitate has a pronounced axial texture along the crystallographic direction <110> perpendicular to the surface of the sample. It can be assumed that the variation of the parameters (amplitude and duration) of current pulses in the forward and reverse directions will affect the degree of orientation of the ordering copper crystallites.

It is known that submicron sizes of crystallites, microstresses and defective structure lead to the expansion of diffraction lines of the

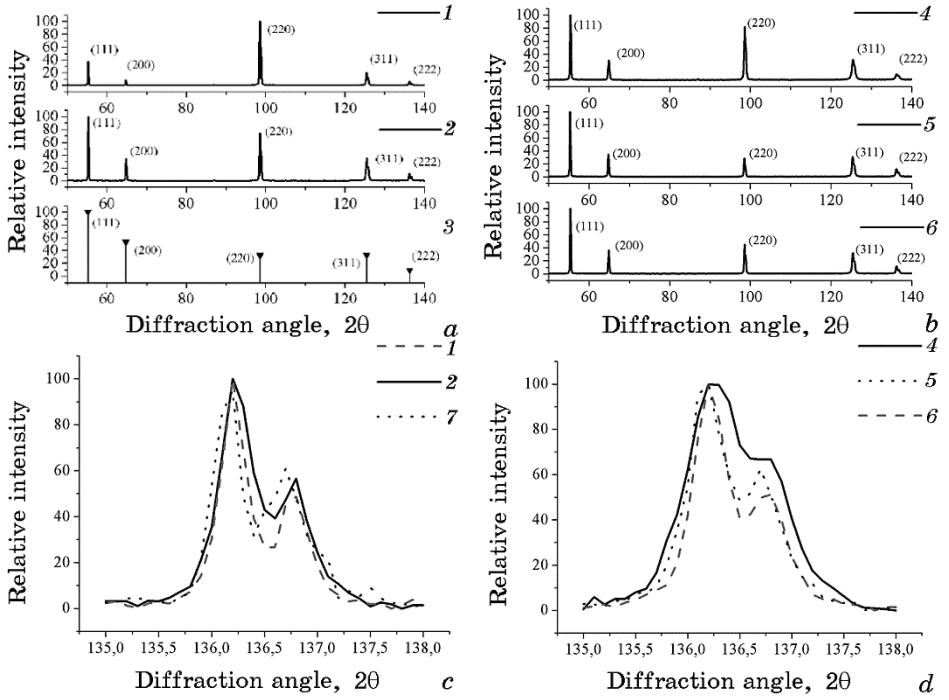

Fig. 4. Diffractograms of the samples with different modes of the copper electrodeposition for diffraction angles: *a*, *b*—50°–140°, *c*, *d*—135°–138°; *1*—Sample 5; *2*—Sample 1; *3*—Standard (bar chart of the PDF-2 database); *4*—Sample 2; *5*—Sample 4; *6*—Sample 3; *7*—Standard (annealed copper powder).

sample. Figure 4, *b* shows the high-rise peak (222) of electrolytic precipitates, obtained by the direct deposition current (Sample 1), for the reverse pulsed mode in comparison with the standard (annealed copper powder). It is clear by the degree of 'splitting' of the K_α doublet that a more perfect structure has a precipitate obtained in reverse pulsed mode. Crystals with defective structure are formed at constant current of electrodeposition.

2.4. The Procedure of Obtaining and Diffusion Annealing of Samples

After electrolytic precipitation of copper, the obtained plates were washed from the residual electrolyte and dried. Before immersion, the copper plates were heated to about 100°C and treated with commercial resin soft activated flux (Weld Team Decapant Liquid, Lincoln Electric Group) to prevent the formation of oxides on the sample surface. The samples were immersed in molten tin at 250°C for about 1 second. The diffusion annealing of the samples was carried out in the Ar atmos-

TABLE 2. Relative intensities of diffraction maxima electrodeposited copper layers.

Crystallographic indices of families of atomic planes (Miller's indices)	(111)	(200)	(220)	(311)	(222)
Sample 1	100	34	74	35	10
Sample 2	100	30	82	31	8
Sample 3	100	36	44	32	11
Sample 4	100	34	28	30	11
Sample 5	37	9	100	20	6
Standard (annealed copper powder)	100	43	30	57	21
Standard (bar chart of the PDF-2 database)	100	43	17	16	5

phere at a temperature of 210°C for 190 hours.

3. CHARACTERIZATION OF SAMPLE CONTACT ZONE

The following characteristics of Cu–Sn samples after diffusion annealing are compared.

1. The average thicknesses of the continuous layers of the η-Cu_6Sn_5 and ε-Cu_3Sn phases were determined by dividing the corresponding total area of the REM images, occupied by the phase, by the total length of the contact surface.

2. To characterize the roughness of the boundary, the following statistical parameters were used: R_q—root mean squared (the mean square value of the deviation profile by the coordinate y from the middle line, which is parallel to the x-axis),

$$R_q = \sqrt{\frac{1}{n}\sum_{i=1}^{n} \Delta y_i^2}, \tag{1}$$

$$\Delta y_i = y_i - \bar{y}; \tag{2}$$

R_v—maximum valley depth,

$$R_v = \min \Delta y_i; \tag{3}$$

R_p—maximum peak height,

$$R_p = \max \Delta y_i; \tag{4}$$

R_{sk}—skewness,

$$R_{sk} = \frac{1}{nR_q^3}\sum_{i=1}^{n}\Delta y_i^3\ ; \tag{5}$$

R_{ku}—kurtosis,

$$R_{ku} = \frac{1}{nR_q^4}\sum_{i=1}^{n}\Delta y_i^4\ ; \tag{6}$$

λ—the average period of the profile inequalities,

$$\lambda = 2\frac{L}{N_{\text{Change}}}, \tag{7}$$

where N_{Change}—the number of changes in deviation sign Δy_i relative to the middle line on the interval L. For filtering of high-frequency transitions through the middle line, an anti-aliasing Calman filter was used [30].

3. Average porosity was determined by the ratio of the cross-sectional area of pores dS^{void} to the total area of the phases dS^{phase} on the two-dimensional sections.

4. Percentage of pores on interface (pores on the interface are most dangerous for strength of contact).

5. Number of pores per unit of length.

6. Distribution of pores along the interface $\rho(\Delta x) = dN^{\text{void}}/d\Delta x$ or, more precisely, the distribution of distances between adjacent pores.

7. Distribution of the number of pore centres perpendicular to the interface $\rho(y) = dN^{\text{void}} / dy$.

8. Distribution of the cross-sectional area of pores perpendicular to the interface $\rho_S(y) = dS^{\text{void}} / dy$.

4. RESULTS AND DISCUSSION

4.1. Characteristic SEM Images of the Contact Area after Annealing

We analyse the surface images of the samples obtained using a raster electron microscope for the presence of characteristic structural elements of the sample diffusion zone, namely, phase boundaries and thicknesses, pore availability and distribution.

It should be noted that the usual polishing modes with diamond and corundum paste do not allow obtaining the sample surface being suitable for porosity analysis due to the high plasticity of copper and the corresponding rubbing of these pores even with finely dispersed pastes. The visualization of the undistorted interphase boundaries and defect boundaries became possible after the procedure of ion-plasma cleaning of the annealed samples.

Pretreatment of SEM images was carried out by Gaussian and Unsharp blurring methods according to the procedures described in [31]. In Ref. [31], algorithms for pretreatment images using appropriate matrix filters have been developed to improve the identification of the boundaries of structural elements, analysis of different types of structural elements (calculating the phase areas and finding the number and calculating the size of structural defects). The presence of white noise in SEM images affects the determination of boundary positions of structural elements of the diffusion zone. First, the Gaussian blurring

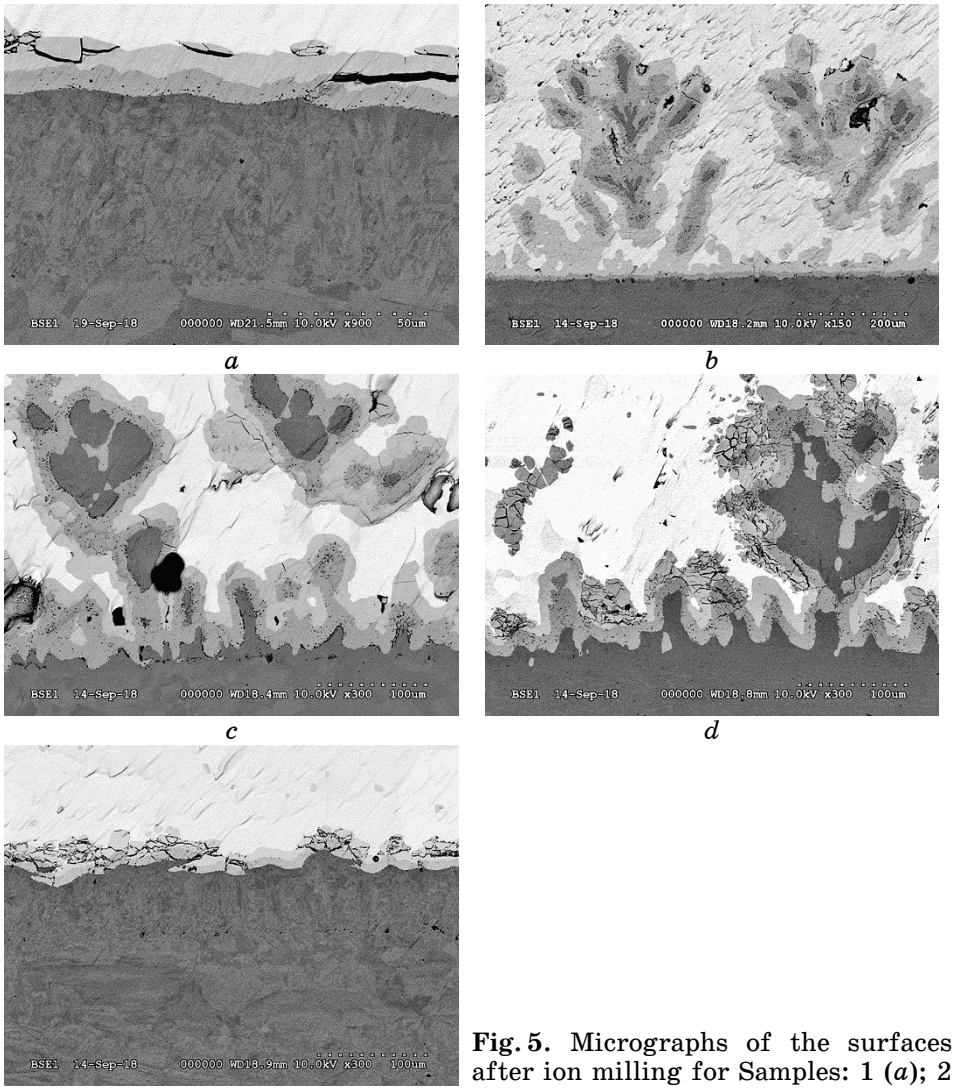

a *b* *c* *d* *e*

Fig. 5. Micrographs of the surfaces after ion milling for Samples: 1 (*a*); 2 (*b*); 3 (*c*); 4 (*d*); 5 (*e*).

method was used to get rid of noise in grey colour gradients; the method averages the value of grey colour gradient in pixels of the image concerning their surroundings, which makes it possible to improve the result of calculating the positions of the interphase boundaries. At the next stage of sample image processing, a method of Unsharp-blurring of the image elements was used that improved the identification of topological defects (Fig. 5). Here, due to the increase of local contrast, as a result of the application of Unsharp-blurring method, the accuracy of the analysis of voids and pores in SEM images increases as the boundaries of these defects on SEM images become more contrasting.

The common characteristic feature of the most samples is the large roughness of the original surface, which most likely leads to a significant distortion of interphase boundary in the process of solid phase reactions and even the separation of a significant proportion of intermetallics (spalling). This is especially true for coatings obtained in stochastic modes and at high densities of deposition currents. It should be noted that determining phase thickness and other characteristics of the contact zones, only the areas forming the percolation cluster were taken into account. In this case, the isolated islands of intermetallics that were 'immured' in the tin matrix were not taken into account in the calculation of characteristics.

4.2. Analysis of Diffusion Zone and Statistical Dependence of Pores along and across the Interface

To analyse the porosity of phase layers for Samples 1–5, the averaged statistical parameters presented in Table 3 were calculated.

Average radius of voids was similar for all samples as it is indicated in the Table 3. With increase of the current density, the average distance between voids and Cu/Cu_3Sn interface increases. This distance is particularly large in samples obtained from stochastic precipitation regimes. The reason may consist in the fact that, in these modes, dislocation density of the copper substrate is greater, *i.e.*, the K-sinks can delay a significant part of nonequilibrium vacancies, thereby, impoverishing the portions of the phase region near the boundary.

TABLE 3. Averaged statistical parameters of porosity phase layers after annealing in a solid phase at 210°C for 190 hours.

Name	Sample 1	Sample 2	Sample 3	Sample 4	Sample 5
Average radius of pores, μm	0,25	0,29	0,25	0,26	0,23
Average distance from pores to interface Cu/Cu_3Sn, μm	1,94	2,98	5,72	3,96	2,41

4.2.1. Average Thicknesses of Continuous Layers of Phases η-Cu_6Sn_5 and ε-Cu_3Sn

While measuring and analysing phase layer thicknesses theoretically, one should consider the following parameters: a substantial part of the reaction takes place for a short period of time during which the solid copper interacts with the liquid tin. In this case, the main growing phase is the scallop-like Cu_6Sn_5 phase. If the interface were flat, the phase thickness would be determined by the rate of supplying copper to the molten tin through the channels between the scallops [3].

$$R = \sqrt[3]{\frac{9}{2}\frac{D\delta(C^b - C^e)}{C_i}t}, \tag{8}$$

where $D = 10^{-9}$ m^2/s [8], $\delta = 2.5 \cdot 10^{-9}$ m [8], $(C^b - C^e) = 8.75 \cdot 10^{-3}$ [8], $C_i = 6/11$ [8], $t = 2$ s.

In the latter formula, 2 seconds instead of 1 second is taken as a reaction time (the time of the very immersion), since the tin remains liquid for some time after taking the sample out. In the mode of solid-phase diffusion in the copper/tin system, the kinetics of phase growth should be determined by the equations derived from the equations of flow balance in the case of plane interphase boundaries [8]. According to the results of work [8], one could expect the ratio of phase thickness to the order of one in the case of solid-phase diffusion annealing. The calculated phase thicknesses are shown in Table 4.

As we can see, the thickness of two phases is about ten microns, which is much greater than the estimate of Cu_6Sn_5 phase thickness immediately after the liquid phase reaction. It means that the initial stage of the reaction can be neglected in this case. The ratio between phase thicknesses is really close to one in four cases of five modes except for the stationary mode with high current density, when Cu_6Sn_5 phase thickness exceeds Cu_3Sn phase thickness almost by three times. In addition, in the fast stochastic mode (Sample 4), Cu_6Sn_5 phase

TABLE 4. Averaged thicknesses of phase layers after annealing in a solid phase at 210°C for 190 hours.

Name	Cu_3Sn, μm	Cu_6Sn_5, μm
Sample 1	6.5	9.5
Sample 2	9.2	26.1
Sample 3	13.2	15.1
Sample 4	9.8	6.2
Sample 5	7.9	8.7

thickness is almost 1.5 times less than Cu_3Sn. This is due to the waviness of the source interface and further fitting of the protrusions to the formation of the isolated islets of Cu_6Sn_5 phase, which are not taken into account in the integral thickness of the layers.

4.2.2. Roughness

The roughness parameters of Cu/Cu_3Sn interface for Samples 1–5 are shown in Table 5.

Table 5 shows that the samples (Sample 3 and Sample 4) obtained in stochastic modes have the highest values of height difference in respect to the middle line (parameters R_v, R_p) as well as the mean square profile (R_p) of the profile deviation (the mean square of absolute values of the profile deviations from the middle line). In Samples obtained in stationary modes, the asymmetry coefficient (R_{sk}) is negative that means that the absolute values of hollow depths are slightly larger than the absolute values of peak heights. Samples 4 and 5 have the narrowest distributions of absolute profile deviations from the middle line (R_{ku}). The average step of the profile λ irregularities in the case of stochastic modes of electrodeposition was less than in stationary and reverse pulsed modes. This seems one of the reasons of additional spalling.

4.2.3. Average Porosity

Average porosity samples after five deposition modes and after further reactions is presented in Fig. 6.

Consequently, the ratio of pore total area to the cross-sectional area of intermetallics proves to be maximal for the maximum deposition current. When decreasing the deposition current, this porosity decreases, if both stochastic regimes are not taken into account. The possible is an interrelation between grain size and the density of the void nucleation sites. The grain size becomes smaller in copper coating with

TABLE 5. Statistical parameters of the interface roughness phase layers after annealing in the solid phase at 210°C for 190 hours.

Name	R_q, μm	R_v, μm	R_p, μm	R_{sk}	R_{ku}	λ, μm
Sample 1	1.5	3.2	3.1	–0.05	2.31	23.5
Sample 2	2.4	5.5	3.7	–0.23	1.98	83.5
Sample 3	8.6	12.5	19.3	0.57	2.04	7.4
Sample 4	9.1	14.1	25.2	0.87	3.48	3.9
Sample 5	3.5	8	8.6	0.49	3.9	31.9

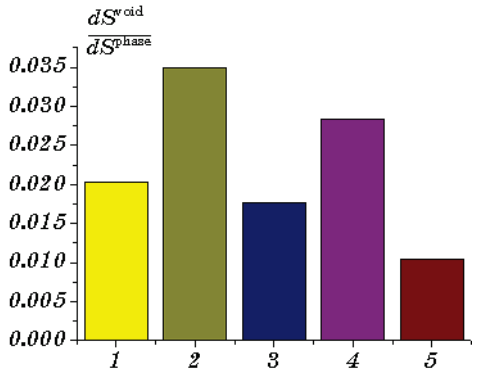

Fig. 6. Average porosity of samples.

larger density of deposition current. Therefore, the density of possible centres of pore formation—triple joints of grain boundaries with the Cu/Cu_3Sn interface becomes larger. As we can see below, the effective voltage in pulse reverse mode is lower than in stationary modes. Therefore, it is clear that, in this mode, one should expect larger grain sizes and, consequently, lower density of joints and less porosity.

4.2.4. Percentage Ratio of Pore Number on Cu/Cu_3Sn Interface

The relative proportion of pores contained in the moving interface of Cu/Cu_3Sn is shown in Fig. 7. In Ref. [15], the theory of kinetic pinning of pores on the mobile interface of Cu/Cu_3Sn was proposed as an additional factor to Ziner pinning by capillary forces. The idea is that the gradient of vacancy concentration in Cu_3Sn phase creates an additional driving force in the process of approaching a pore to the interface. This gradient depends on the defect of copper matrix, more precisely, on the

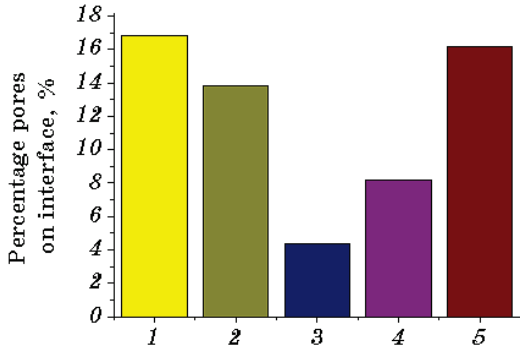

Fig. 7. Percentage of pores on interface.

density of dislocation sinks in copper, which depends on pretreatment. In Ref. [15], the following conclusion was made: 'More defects, less pinning'. The same picture is observed in comparing modes 1 and 2. This rule seems to be applied in the case of stochastic deposition modes.

4.2.5. Number of Pores per Unit of Length

To determine the number of pores per unit of length of the interface, the average distance between the pores along the interface was initially calculated, and the value of $l = 1 / \bar{l}$ was then found. This parameter has a clear physical content only for the relatively small roughness of the interface observed after the deposition in modes 1, 2, 5. Here, for better comparison, we introduced an effective voltage for mode 5:

$$U_{\text{ef}} = \frac{U^+ t^+ - U^- t^-}{t^+ + t^-}. \tag{9}$$

According to our parameters $U^+ = 0.367$ V, $U^- = 0.119$ V, $t^+/t^- = 2$, we get $U_{\text{ef}} = 0.205$ V. The results of comparison are presented in Table 6. We see that there is approximately a linear empirical relationship between the applied effective voltage during the deposition and the number of pores per unit of length of the interface.

$$\frac{1}{\bar{l}} \approx kU. \tag{10}$$

We did not include the samples obtained in stochastic modes (Sample 3 and Sample 4) in the present analysis, since it is difficult to speak about the x-axis as a measure of displacement along the interface in these samples. As we can see from the SEM images mentioned above, the total length of bends is greater than the length of the interface along the x-axis.

4.2.6. Distribution of Pores along the Interface

Ideally, if the interface was flat and the origin of pores on this inter-

TABLE 6. Dependence of pore density on effective voltage for non-stochastic regimes.

Name	Sample 1	Sample 2	Sample 5
U_{ef}	0.24 V	0.49 V	0.205 V
$1 / \bar{l}$	0.75 μm^{-1}	1.23 μm^{-1}	0.59 μm^{-1}
$(1 / \bar{l}) / U$	3.1 $\mu m^{-1} V^{-1}$	2.5 $\mu m^{-1} V^{-1}$	2.9 $\mu m^{-1} V^{-1}$

face was completely random, one would expect the Poisson distribution for the histogram of distance distribution between the pores:

$$\rho(\Delta x) = \rho_0 \exp\left(-\frac{\Delta x}{\lambda}\right). \quad (11)$$

If pores like some places of the interface more than others, that is, if there are certain areas of more favourable pore formation, the distribution can be, for example, two-mode one:

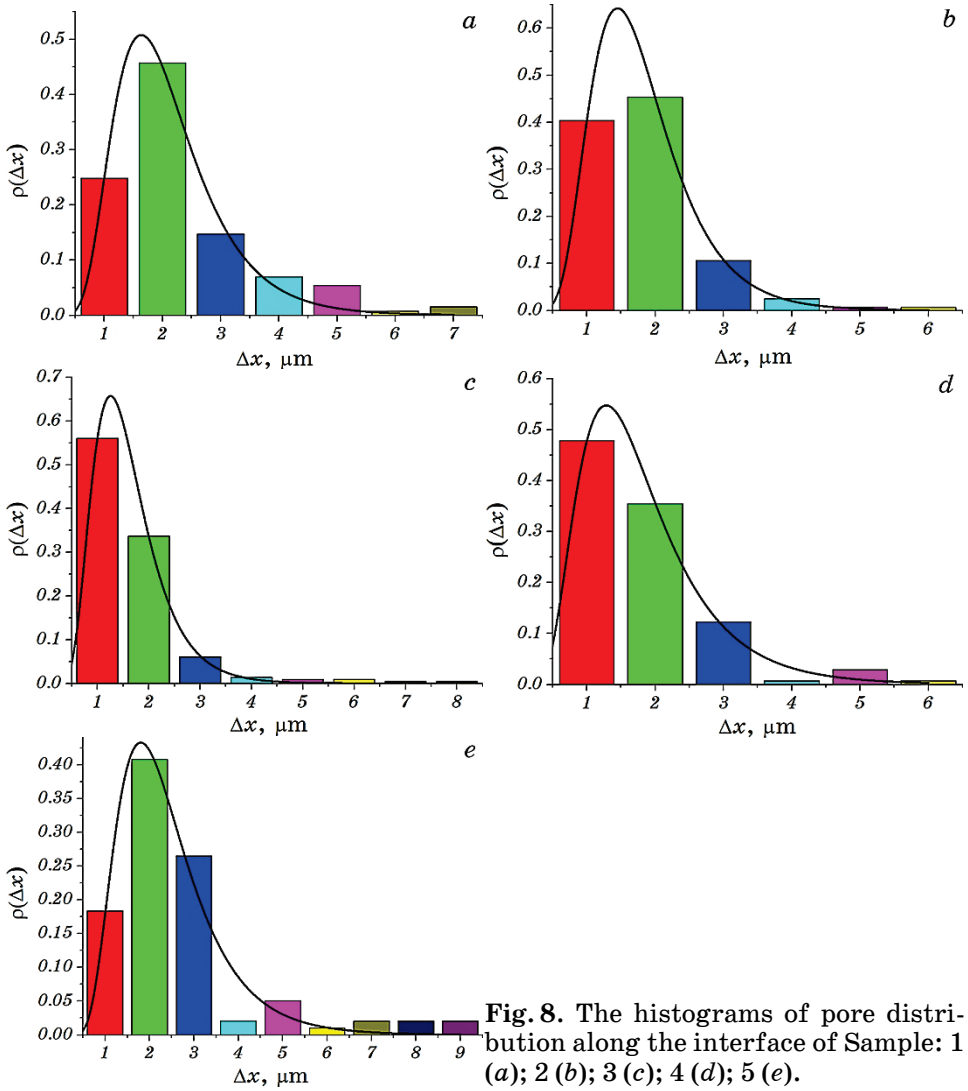

Fig. 8. The histograms of pore distribution along the interface of Sample: 1 (*a*); 2 (*b*); 3 (*c*); 4 (*d*); 5 (*e*).

$$\rho(\Delta x) = \rho_{10} \exp\left(-\frac{\Delta x}{\lambda_1}\right) + \rho_{20} \exp\left(-\frac{\Delta x}{\lambda_2}\right). \quad (12)$$

The obtained results show that, the approximation by lognormal distribution fits more than the Poisson one, especially for non-monotonic histograms.

The histograms in Fig. 8 show that distance distributions are very far from the Poisson one, and therefore, the formation of pores on the interface is a correlated effect.

4.2.7. Distribution of the Number of Pore Centres Perpendicular to the Interface

In virtually all cases, the peak of pore distribution is fixed directly at the interface itself, indicating the pore pinning by the moving interface.

4.2.8. Distribution of the Cross-Sectional Area of Pores Perpendicular to the Interface

A similar picture is observed for the distributions of both pore areas and pore centres (Fig. 9), *i.e.*, there is not only maximum percentage of pore centres, but also the maximum percentage of pore cross sections near the interfaces (Fig. 10). That is, the pores near the interface are also quite large.

In the case of small deposition current, most of all pores are located near the interface, and in the case of stochastic modes, the number of pores in the middle of intermetallic layers significantly exceeds the number of pores on the interface.

5. CONCLUSIONS

The hypothesis about the influence of pretreatment of the rolled copper plates by using various modes of electrodeposition of copper on them, on the defect of the contact zone after solid-phase copper–tin reactions is tested.

The peculiarity of the conducted research is the use of not only deposition modes with constant or periodic current, but also the implementation of fast and slow stochastic modes implemented by the developed hardware and software complex. The stochastic modes of electrodeposition were obtained on the basis of the Chua generator model of random oscillations at two stationary points. Stationary states were selected from the analysis of polarization curve according to the condi-

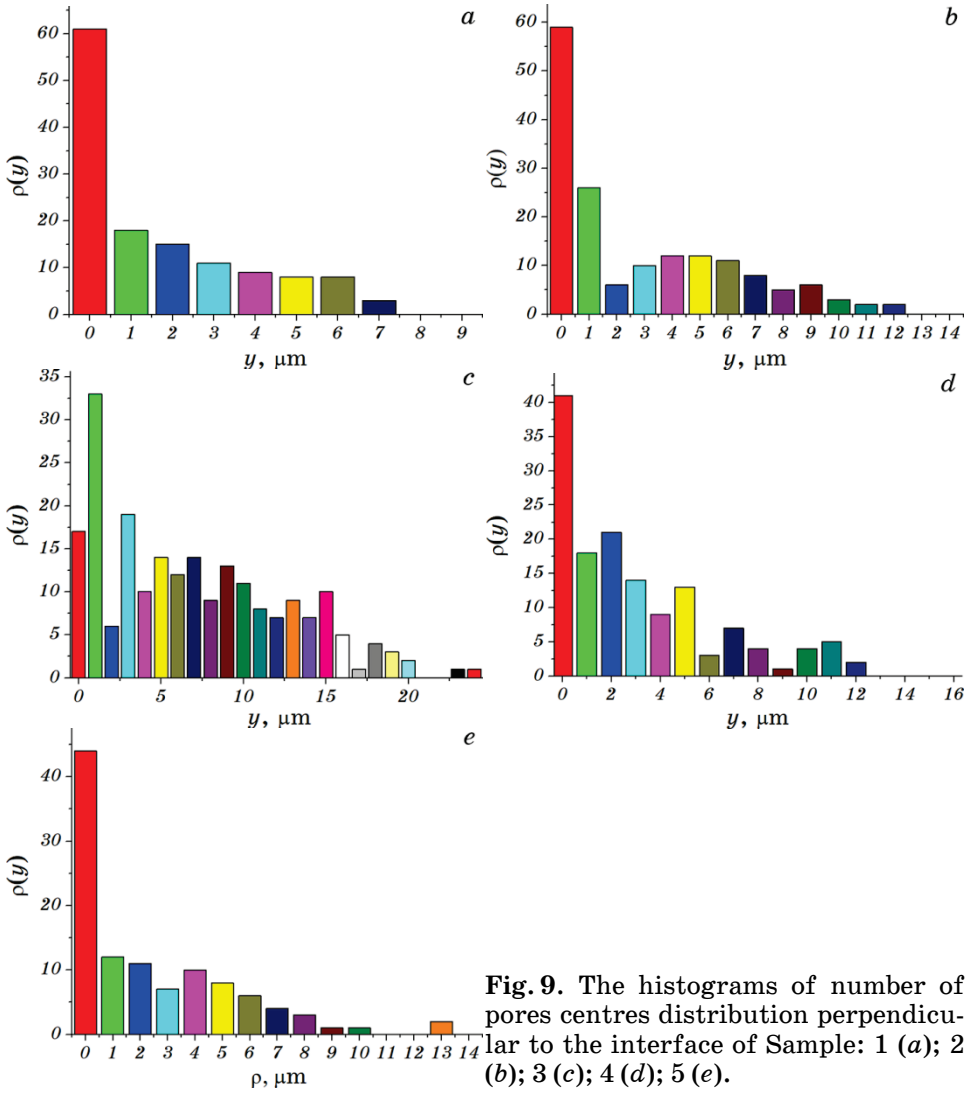

Fig. 9. The histograms of number of pores centres distribution perpendicular to the interface of Sample: 1 (*a*); 2 (*b*); 3 (*c*); 4 (*d*); 5 (*e*).

tions of electrodeposition.

So, there are results as follow.

1. The following regularity is confirmed: the higher the electrodeposition current density, the greater the defect of coating and the greater the porosity of Cu_3Sn phase occurring during the solid phase reaction between copper and tin.

2. In particular, the number of pores per unit of length of the interface is approximately proportional to the voltage during depositing copper on copper.

3. The percentage of pores addicted to moving interface also depends

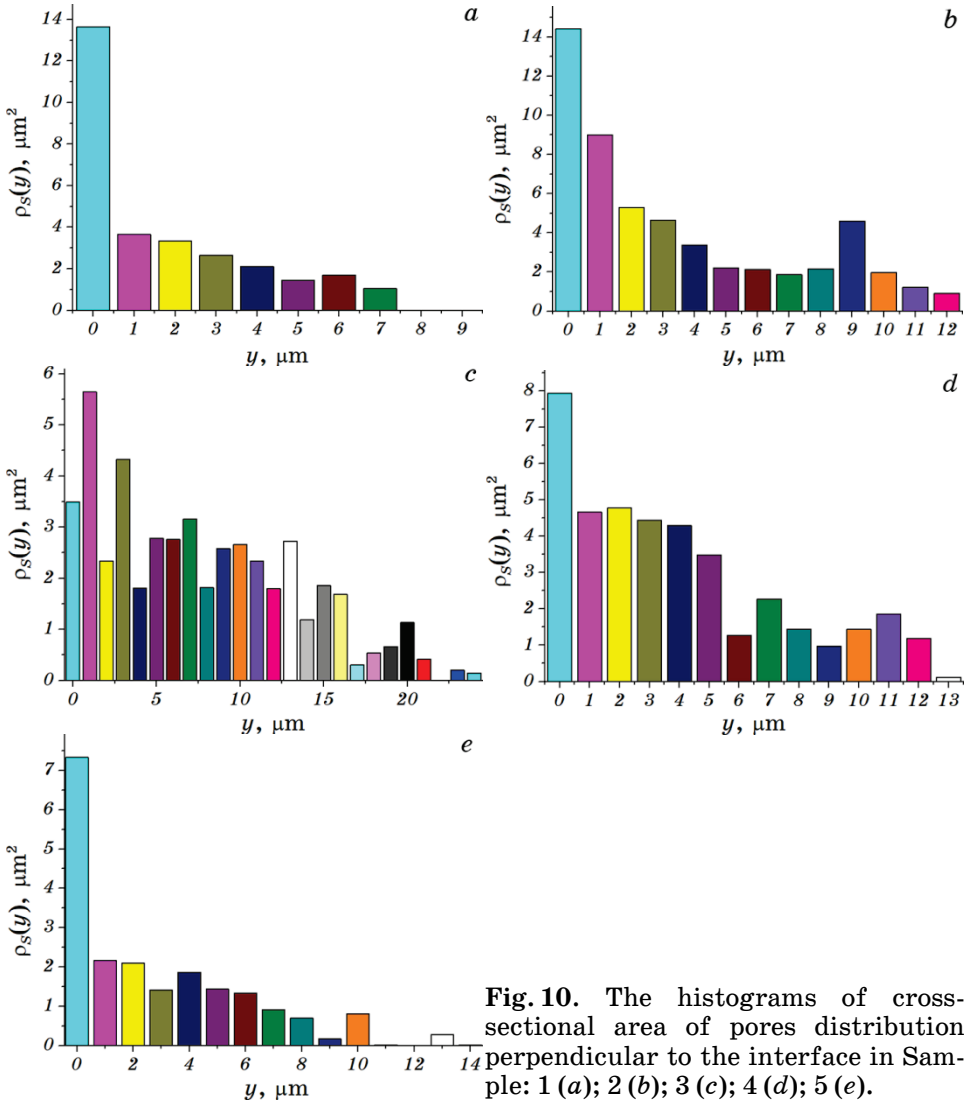

Fig. 10. The histograms of cross-sectional area of pores distribution perpendicular to the interface in Sample: 1 (*a*); 2 (*b*); 3 (*c*); 4 (*d*); 5 (*e*).

on the defect. This confirms the hypothesis of work [15]: 'More defects, less pinning'.

4. The distance distribution between pores does not correspond to Poisson one and is well approximated by the lognormal distribution, which indicates the correlation of pore formation in different places.

5. The distribution of pores by distances from the interface is determined for the first time. It shows an abnormal accumulation of pores on the interface itself or at a short distance from it. The corresponding analytic approximation will be discussed in further paper.

6. The mechanical strength of the contact is determined by not only the thickness of phase layers but also the roughness and geometry of the interface. It is quite possible that the abnormal roughness obtained by stochastic modes can significantly affect the strength with respect to the directed loads.

ACKNOWLEDGEMENTS

The authors gratefully acknowledge financial support from the Ministry of Education and Science of Ukraine (state registration number: 0117U000577). The work is also partly supported by the European project EXMONAN EU Marie Curie FP7 (Grant # 612552).

REFERENCES

1. K. N. Tu, *Electronic Thin-Film Reliability* (Cambridge University Press: 2010).
2. K. N. Tu, *Solder Joint Technology* (New York: Springer: 2007).
3. A. M. Gusak and K. N. Tu, *Phys. Rev. B*, **66**, No. 11: 115403 (2002).
4. K. M. Tu, A. M. Gusak, and M. Li, *J. Appl. Phys.*, **93**, No. 3: 1335 (2003).
5. J. O. Suh, K. N. Tu, G. V. Lutsenko, and A. M. Gusak, *Acta Mater.*, **56**, No. 5: 1075 (2008).
6. O. Yu. Liashenko and F. Hodaj, *Acta Mater.*, **99**: 106 (2015).
7. O. Yu. Liashenko, S. Lay, and F. Hodaj, *Acta Mater.*, **117**: 216 (2016).
8. O. Yu. Liashenko, A. M. Gusak, and F. Hodaj, *J. Mater. Sci.: Mater. Electron.*, **25**, No. 10: 4664 (2014).
9. Ya. E. Geguzin, N. Ch. Bao, and L. N. Paritskaya, *Fiz. Met. Metalloved.*, **27**, No. 3: 450 (1969) (in Russian).
10. Ya. Ye. Geguzin, *Diffuzionnaya Zona* [Diffusion Zone] (Moscow: Nauka: 1979) (in Russian).
11. A. M. Gusak, and N. V. Storozhuk, *Phys. Metals Metallogr.*, **114**, No. 3: 197 (2013).
12. T. V. Zaporozhets, N. V. Storozhuk, and A. M. Gusak, *Metallofiz. Noveishie Tekhnol.*, **38**, No. 10: 1279 (2016).
13. Y. W. Wang, Y. W. Lin, and C. R. Kao, *Microelectronics Reliability*, **49**, No. 3: 248 (2009).
14. T.-C. Liu, C.-M. Liu, Y.-S. Huang, C. Chen, and K.-N. Tu, *Scr. Mater.*, **68**, No. 5: 241 (2013).
15. A. M. Gusak, T. V. Zaporozhets, and J. Janczak-Rusch, *Philos. Mag. Lett.*, **97**, No. 1: 1 (2017).
16. Yu. V. Nikolenko, V. A. Diduk, Ya. D. Korol, and Yu. O. Lyashenko, *Bulletin of Cherkasy University. Series 'Physics and Mathematics'*, **1**: 26 (2016) (in Ukrainian).
17. V. M. Tyutenko, V. V. Morozovych, V. A. Diduk, S. O. Kolinko, and Yu. O. Lyashenko, *Bulletin of Cherkasy University. Series 'Physics and Mathematics'*, **1**: 63 (2017) (in Ukrainian).
18. *Elektroosazhdenie Metallicheskikh Pokrytiy: Spravochnik* [Electrodeposition of Metallic Coatings: Handbook] (Eds. M. A. Belenkiy and A. F. Ivanov) (Moscow:

Metallurgiya: 1985) (in Russian).
19. K. I. Popov, S. S. Djokić, N. D. Nikolić, and V. D. Jović, *Morphology of Electrochemically and Chemically Deposited Metals* (Switzerland: Springer: 2016).
20. A. A. Medvedev and S. Semenov, *Tekhnologii v Elektronnoy Promyshlennosti*, **3**: 68 (2005) (in Russian).
21. M. Kapitsa, *Tekhnologii v Elektronnoy Promyshlennosti*, **2**: 20 (2006) (in Russian).
22. A. B. Kilimnik, *Vestnik TGTU*, **14**, No. 4: 903 (2008) (in Russian).
23. Z. Stevich, M. Raychich-Vuyasinovich, and Z. Stoilkovich, *Tekhnologiya i Konstruirovanie v Elektronnoy Apparature*, **5**: 51 (2003) (in Russian).
24. D. Yu. Ushchapovskiy, O. V. Linyucheva, M. I. Donchenko, M. V. Bik, and A. S. Tsimbalyuk, *Naukovi Visti NTUU 'KPI'*, **2**: 114 (2016) (in Ukrainian).
25. V. T. Hrynchenko, V. T. Matsypura, and A. A. Snarskyy, *Vvedeniye v Nelineynuyu Dinamiku. Khaos i Fraktaly* [Introduction to Nonlinear Dynamics. Chaos and Fractals] (Moscow: LKI: 2007) (in Russian).
26. L. Chua, *IEEE Transactions on Circuits and Systems*, **27**, No. 11: 1059 (1980).
27. T. A. Matsumoto, *IEEE Transactions on Circuits and Systems*, **31**, No. 12: 1055 (1984).
28. G. Wassermann and J. Grewen, *Tekstury Metallicheskikh Materialov* [Textures of Metallic Materials] (Moscow: Metallurgiya: 1974) (Russian translation).
29. S. M. Kochergin and A. V. Leontiev, *Obrazovanie Tekstur Pri Elektrokristallizatsii Metallov* [Texture Formation During Electrocrystallization of Metals] (Moscow: Metallurgiya: 1974) (in Russian).
30. M. S. Grewal and A. P. Andrews, *Kalman Filtering—Theory and Practice Using MATLAB* (Wiley: 2001).
31. V. V. Morozovych, A. R. Honda, and Yu. O. Lyashenko, *Bulletin of Cherkasy University. Series 'Applied Mathematics. Computer Science'*, **1**: 14 (2017) (in Ukrainian).